REPORT DOCUMENTATION PAGE

Form Approved
OMB No. 0704-0188

1. AGENCY USE ONLY *(Leave blank)*	2. REPORT DATE	3. REPORT TYPE AND DATES COVERED
	17 August 1998	

4. TITLE AND SUBTITLE
Upper Atmospheric Modeling for Mars Global Surveyor Aerobraking Using Least Squared Processes

5. FUNDING NUMBERS

6. AUTHOR(S)
Brandon Wilkerson

7. PERFORMING ORGANIZATION NAME(S) AND ADDRESS(ES)
George Washington University

8. PERFORMING ORGANIZATION REPORT NUMBER
98-003 Major Report

9. SPONSORING/MONITORING AGENCY NAME(S) AND ADDRESS(ES)
THE DEPARTMENT OF THE AIR FORCE
AFIT/CIA, BLDG 125
2950 P STREET
WPAFB OH 45433

10. SPONSORING/MONITORING AGENCY REPORT NUMBER

11. SUPPLEMENTARY NOTES

12a. DISTRIBUTION AVAILABILITY STATEMENT
Unlimited distribution
In Accordance With 35-205/AFIT Sup 1

12b. DISTRIBUTION CODE

13. ABSTRACT *(Maximum 200 words)*

14. SUBJECT TERMS

15. NUMBER OF PAGES
22

16. PRICE CODE

17. SECURITY CLASSIFICATION OF REPORT	18. SECURITY CLASSIFICATION OF THIS PAGE	19. SECURITY CLASSIFICATION OF ABSTRACT	20. LIMITATION OF ABSTRACT

Standard Form 298 (Rev. 2-89) (EG)
Prescribed by ANSI Std. 239.18
Designed using Perform Pro, WHS/DIOR, Oct 94

Upper Atmospheric Modeling for Mars Global Surveyor Aerobraking Using Least Squared Processes

Brandon Wilkerson
B.S. Engineering Sciences, US Air Force Academy, 1996
M.S. Mechanical Engineering, George Washington University, 1998

April 20, 1998

Abstract

Mars Global Surveyor (MGS) will be performing an aerobraking maneuver to move from its highly elliptical initial orbit to its final nearly circular mapping orbit. This maneuver will occur from September 1997 to approximately September 1998. To accomplish this maneuver safely and quickly, it will be necessary to accurately know the atmospheric environment at aerobraking altitudes (approximately 100-140 kilometers above the surface of the planet). One way of accomplishing this is by using accelerometer data from the spacecraft. The method of least squares is used to fit density measurements determined from the accelerometer data, which results in an empirical model that characterizes the atmosphere. This can be done by breaking the data up into regions of interest or by taking the entire data set, resulting in different types of atmospheric information. The hydrostatic equation is the governing equation for the models assuming three different temperature profiles: constant, linear, and Bates. The least squares solution yields information about density, temperature, scale height, pressure, and atmospheric variability. This information is fed back to the navigation team and the atmospheric advisory group to aid in the orbital correction decision making process. Also, this information will be compared over time to determine latitudinal, diurnal, and seasonal trends in the Martian atmosphere. This will lead to a more accurate atmospheric model than those currently being used.

Table Of Contents

Table Of Figures

List of Symbols and Variables

A - A Matrix
α - latitudinal variation gradient
g or g(z) - acceleration due to gravity
g_0 - acceleration due to gravity at the surface of Mars (3.4755 m/sec^2)
H_s - scale height
k - Boltzman's constant (1.381×10^{-23} J/K*molecule)
L - latitude
L_0 - reference latitude
LV - latitudinal variation
m - mean molecular weight
m_i - mean molecular weight for ith specie
n_i - number density for ith specie
p - pressure
R - universal gas constant (8.314 J/K*mole)
ρ - density
ρ_0 - base density
R_m - radius of mars (3393 km)
s_1 - shape factor above inflection point
s_2 - shape factor below inflection point
T - temperature Profile
T_I - temperature at inflection point
T_∞ - exospheric temperature
T_L - lower atmospheric temperature
T_0 - base temperature
T_1 - temperature increase (K/km)
z - altitude
z_0 - base altitude

Section 1: Introduction

The Mars Global Surveyor spacecraft (MGS) was launched on 7 November 1996 and reached Mars on 12 September 1997. Upon reaching Mars, Surveyor fired its main rocket engine for the Mars orbit insertion (MOI) burn which slowed the spacecraft and allowed it to be captured into orbit by the planets gravity field. The initial orbit was a highly elliptical orbit with a 48 hour period. After MOI, the periapsis altitude was decreased to about 110-150 kilometers by another attitude control system burn. At these altitudes, MGS will encounters air resistance causing the satellite to lose energy. This energy loss causes the spacecraft's apoapsis altitude to decrease on successive orbits. This "aerobraking" technique is planned to drop the apoapsis altitude from around 56,000 km to about 400 km.

Before this mission, there was limited knowledge of the Martian upper atmosphere due to minimal Mars missions in the past twenty years. Upper atmospheric data is limited to the Viking I and II entries in 1976 and the recent Pathfinder entry in July, 1997. This unknown atmosphere posed problems for the MGS mission. During aerobraking, as MGS goes lower and lower into the atmosphere, the spacecraft is subject to higher densities which lead to increased aerodynamic heating and dynamic pressure. This can threaten solar panel melting points and structural integrity if encountered atmospheric densities are too large. This situation was encountered around Periapsis 15 when MGS saw a large increase in density due to an atmospheric disturbance. It is believed that the dynamic pressures caused by this high density led to structural damage to one of the solar arrays.

The George Washington University/Joint Institute for the Advancement of Flight Sciences (GWU/JIAFS) accelerometer team uses spacecraft accelerometer data to help characterize the atmospheric conditions MGS encounters. Depending on the amount of accelerometer data received, the data can be conditioned and averaged to give an accurate density vertical structure. A least squares process is then used to determine atmospheric parameters that characterize the atmosphere. These parameters include values such as density, scale height, and temperature.

Due to the near-real time nature of the accelerometer data received by the GWU/JIAFS accelerometer team, these empirical models can be used to immediately predict whether the spacecraft is in danger. For long period orbits, data is received by the GWU/JIAFS accelerometer team about two hours after a periapsis pass. Within eight hours, the accelerometer data is analyzed and feedback is given to mission planners regarding the atmospheric conditions.

Over time, it is possible to use knowledge from these models to predict future atmospheric conditions. Again, this knowledge can be used to ensure spacecraft safety. Finally, these models can be used to gain an understanding of the entire Martian upper atmosphere. MGS presents an opportunity to make hundreds of upper atmospheric "entries." Consequently, these entries give hundreds of different vertical structures at various locations above the planet. Because of this wide range of data, it is possible to study various trends that occur in the atmosphere. Also, because of the aerobraking mission, the data received will go to altitudes lower than any previous

orbiter. Before this mission, the only knowledge of the atmosphere at altitudes near 100 km came from planetary landers. Due to the limited number of landers, knowledge at this altitude level is minimal.

Section 2: Theory

This section will discuss the theory of the mathematics used for the modeling and characterization of the Martian atmosphere. First, the method of least squares will be discussed. This is the technique applied to model the atmosphere using the hydrostatic equation as a basis. The hydrostatic equation is dependent on a temperature profile, so next, the different types of temperature models will be discussed. Much additional information beyond temperature and density can be taken from these models. This additional information will be discussed at the end of this section.

2.1 Least Squares Theory

The method of least squares is a process which compares a model of a data set to the actual data set. By comparing the differences of the two models, it is possible to change the modeled data set to more accurately describe the actual data set. For the Mars atmospheric modeling, this was done using two different methods: linear least squares and non-linear least squares.

2.1.1 Linear Least Squares

The method of least squares is used to model the Martian atmosphere. As an example, suppose we have a set of densities over a certain range of altitudes for an isothermal atmosphere. From the hydrostatic equation, this profile can be expected to follow the model

$$\rho(h) = \rho(h_o)\ \exp\left(-(h-h_o)/H_s\right) \qquad \text{(Section 2: -1)}$$

The derivation of this expression will be discussed further in Section 2.4. It is seen that this is an exponential relationship and plots of ln(ρ) vs. altitude will be linear with the form

$$\ln\rho(h) = \ln\rho_o - (h-h_o)/H_s \qquad \text{(Section 2: -2)}$$

Thus, to characterize this atmosphere, the simplest model would be a line with the form $y_c=mz+b$, where the intercept is ln ρ_o and the slope is $-1/H_s$. Since there will be some measurement error, the observed data can be modeled by the equation

$$y_{oi} = y_{ci} + \varepsilon_i = m z_i + b + \varepsilon_i \quad i = 1....n \qquad \text{(Section 2: -3)}$$

The least square estimate of the unknowns m and b are the values that minimize J, where

$$2J(a,b) \equiv \sum_{i=1}^{n} \varepsilon_i^2 = \sum_{i=1}^{n} \left(y_{oi} - y_c\right)^2 = \sum_{i=1}^{n} \left(y_{oi} - m z_i - b\right)^2$$

(Section 2: -4)

Notice that if J is expanded, it is quadratic in m and b. Since J is non-negative, there is exactly one extremum value for J which is a minimum. The values for m and b that yield this minimum are the values which give the "least square" error. To find the minimum value of J, the following expressions are used:

$$\frac{\partial J}{\partial m} = 0 \qquad \frac{\partial J}{\partial b} = 0 ,$$

(Section 2: -5)

which yield

$$\frac{\partial J}{\partial m} = \left(\Sigma z_i^2\right) m + \left(\Sigma z_i\right) b - \Sigma y_{oi} z_i = 0$$

$$\frac{\partial J}{\partial b} = \left(\Sigma z_i\right) m + nb - \Sigma y_{oi} = 0$$

(Section 2: -6)

The solution to this system of equations is the least squares solution, which expressed in matrix form is

$$\begin{vmatrix} \Sigma z_i^2 & \Sigma z_i \\ \Sigma z_i & n \end{vmatrix} \begin{vmatrix} m \\ b \end{vmatrix} = \begin{vmatrix} \Sigma y_{oi} z_i \\ \Sigma y_{oi} \end{vmatrix} .$$

(Section 2: -7)

In vector-matrix form, Equation 2.1 becomes

$$\mathrm{y}_o = \begin{vmatrix} z_1 & I \\ z_2 & I \\ . & . \\ . & . \\ z_n & I \end{vmatrix} \mathrm{x} + \varepsilon \equiv \mathrm{Ax} + \varepsilon$$

(Section 2: -8)

where y_0, x, and ε are vectors and A is a matrix. The vector x is formed from the unknowns m and b. In this form, Equation 2-7 can be written as

$$A^T Ax = A^T y_o \qquad \text{(Section 2: -9)}$$

which is known as the normal equation. Any vector x that satisfies the normal equations is a least squares solution and is denoted by $\hat{x}$. Thus, the least squares solution can be solved using the expression

$$\hat{x} = \left(A^T A\right)^{-1} A^T y_o \qquad \text{(Section 2: -10)}$$

2.1.2 Non-Linear Least Squares

More complex models are forced to use a nonlinear relationship between the measurements and the model parameters. If we assume a linear temperature profile ($T=T_0+T_1$) instead of an isothermal atmosphere (constant temperature), the model becomes

$$\ln \rho = \ln \rho_0 - \left(1+\tfrac{g}{RT_1}\right)\ln\left(1+\tfrac{T_1}{T_0}\left(z-z_0\right)\right) \qquad \text{(Section 2: -11)}$$

In this expression, there is no longer a simple linear relation. The model parameters are now ln ρ_o, T_0, and T_1. Having to take the natural log of the T_1/T_0 term is what causes a non-linearity and forces the use of iteration by some form of the Newton-Raphson process.

The steps outlined for the linear least squares method are the same for the

$$A^T A\Delta x = A^T\left[y_o - y_c(x_k)\right] \qquad \text{(Section 2: -12)}$$

nonlinear least squares method. However, the normal equation has the form where A is given by

$$A(i,j) = \frac{\partial y_{ci}}{\partial x_j} \qquad \text{(Section 2: -13)}$$

It is necessary to assume y_c for the first iteration. This is done by estimating the model parameters ln ρ_0, T_0, and T_1. This gives the initial estimate for ln ρ which is taken as y_c. Once Δx is determined, the next estimate for x is $x_{k+1}=x_k+\Delta x$. Using this new value of x, the A matrix is calculated and the iteration continues until changes in Δx are small, which is called model convergence.

2.2 Rationale Behind The Models

Based on experience, three different temperature models were chosen to generate atmospheric models. The most basic temperature profile is the constant temperature profile, which is called an isothermal atmosphere. This model was chosen because of its simplicity and trends seen in past Mars descents. Data from the Viking I and II landers shows near isothermal atmospheres as seen in Figure 2.1.

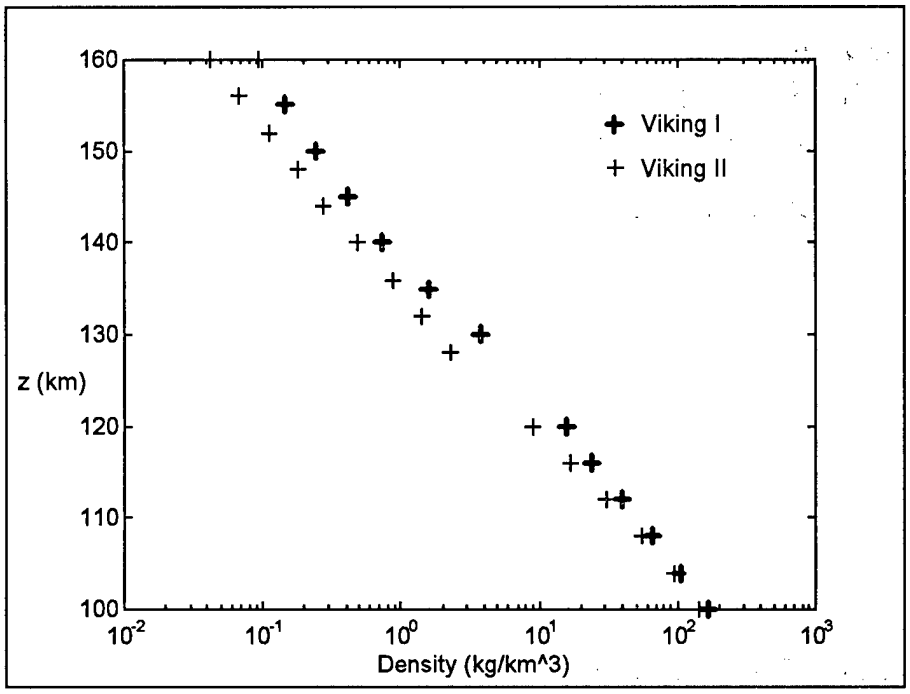

Figure Section 2: .1: Viking Entry Density Data

Based on known atmospheres of Earth and Venus, two other profiles were expected to be encountered. These are the linear temperature profile, and the Bates temperature profile, which was developed by David Bates in 1959 (Bates—see walker paper). These two profiles are shown in Figures 2.2 and 2.3.

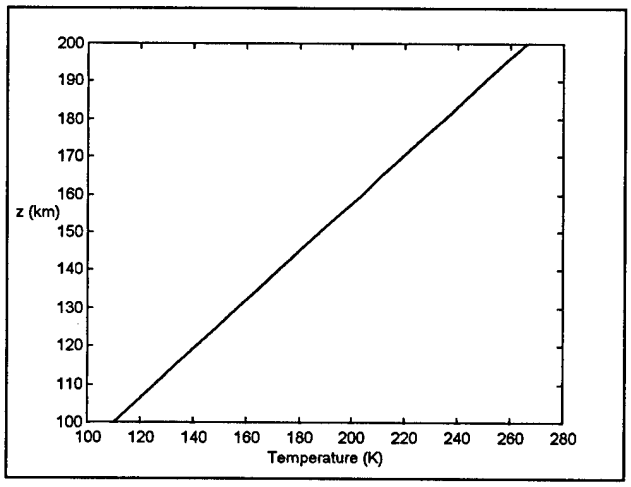

Figure Section 2: .2: Linear Temperature Profile

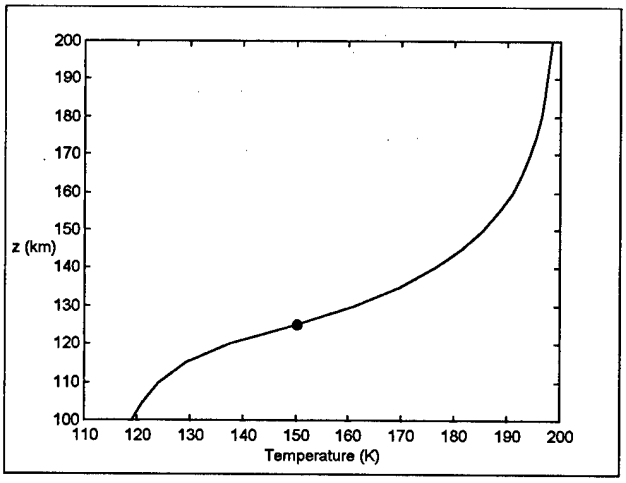

Figure Section 2: .3: Bates Temperature Profile

Once aerobraking began, it was evident that there was often a strong latitudinal gradient in the density profile. This necessitated a latitudinal variation model. A constant temperature latitudinal variation model was created. A comparison of a density profile for a constant temperature model with and without a latitudinal variation is shown in Figures 2.4 and 2.5.

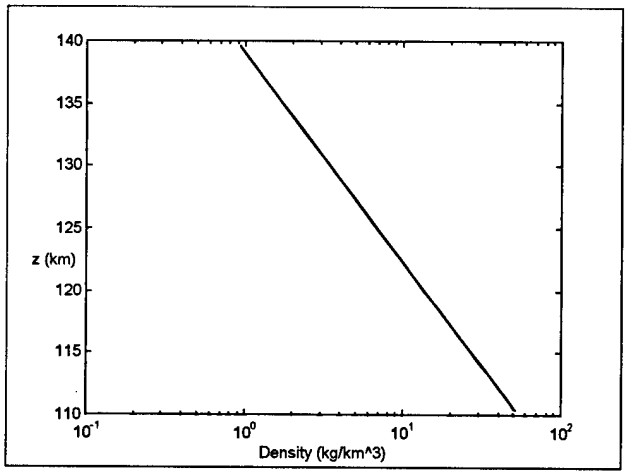

Figure Section 2: .4: No Latitudinal Variation

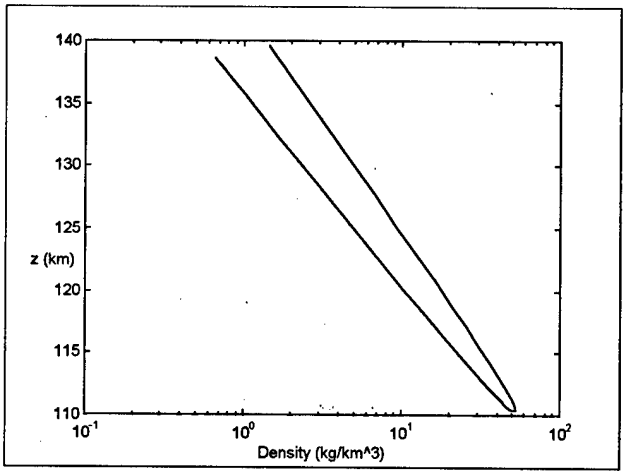

Figure Section 2: .5: With Latitudinal Variation

2.3 Model Derivation

In this section, the expressions for the atmospheric density models are derived. These are the equations that will model the observed data, similar to (2-1) and (2-11) in Section 2.1. To derive these equations, we begin with the hydrostatic equation

$$\frac{dp}{dz} = -\rho g \qquad \text{(Section 2: -14)}$$

and then substitute in the ideal gas equation

$$p = \rho RT \qquad \text{(Section 2: -15)}$$

giving

$$\frac{d}{dz}(\rho RT) = -\rho g . \qquad \text{(Section 2: -16)}$$

The next step is to assume a temperature profile which is substituted into (2-16). The temperature substitution for the three different temperature profiles and the resulting derivations are shown in the following sections.

2.3.1 Constant Temperature Model

Since the temperature and the universal gas constant are constant, (2-16) can be written

$$RT\frac{d\rho}{dz} = -\rho g \qquad \text{(Section 2: -17)}$$

Manipulating this expression, we write

$$\frac{d\rho}{\rho} = -\frac{g}{RT}dz . \qquad \text{(Section 2: -18)}$$

Integrating both sides yields

$$\ln\left(\frac{\rho}{\rho_0}\right) = -\frac{g}{RT}(z - z_0) \qquad \text{(Section 2: -19)}$$

which becomes

$$\ln\rho - \ln\rho_0 = -\frac{g}{RT}(z - z_0). \qquad \text{(Section 2: -20)}$$

Or, solving for ln ρ,

$$\ln\rho = \ln\rho_0 - \frac{g}{RT}(z - z_0) \qquad \text{(Section 2: -21)}$$

This is the same as (2-2), if the scale height H_s is given by the expression

$$H_s = \frac{RT}{g} \qquad \text{(Section 2: -22)}$$

In this model, we have two parameters, H_s and ln ρ_0. Since this is a linear least squares problem, it is not essential to find the A matrix, but the process will be shown. The A matrix is found by taking the partial derivatives of the (2-21) with respect to the parameters, H_s and ln ρ_0. These partials become

$$\frac{\partial \ln\rho}{\partial \ln\rho_0} = 1 \qquad \text{(Section 2: -23)}$$

$$\frac{\partial \ln\rho}{\partial H_S} = -(z - z_0). \qquad \text{(Section 2: -24)}$$

2.3.2 Linear Temperature Model

Assuming a linear temperature profile,

$$T = T_0 + T_1 z \qquad \text{(Section 2: -25)}$$

means the temperature, T, is no longer constant. So, we must take the derivative with respect to T as well as with respect to ρ. Taking the derivative of (2-16) gives

$$T\frac{d\rho}{dz} + \rho\frac{dT}{dz} = -\rho\frac{g}{R}. \qquad \text{(Section 2: -26)}$$

Now substituting (2-25) into (2-26) gives

$$(T_0 + T_1 z)\frac{d\rho}{dz} + \rho\frac{d(T_0 + T_1 z)}{dz} = -\rho\frac{g}{R} \qquad \text{(Section 2: -27)}$$

Carrying out the differentiation on the second term leads to the simplified expression

$$(T_0 + T_1 z)\frac{d\rho}{dz} + \rho T_1 = -\rho\frac{g}{R} \qquad \text{(Section 2: -28)}$$

or

$$(T_0 + T_1 z)\frac{d\rho}{dz} = \rho\left(-T_1 - \frac{g}{R}\right). \qquad \text{(Section 2: -29)}$$

Again, manipulation of this expression gives

$$\frac{d\rho}{\rho} = \frac{\left(-T_1 - \frac{g}{R}\right)}{T_0 + T_1 z} dz \qquad \text{(Section 2: -30)}$$

which is integrated using the expression

$$\int_{\rho_0}^{\rho_1} \frac{d\rho}{\rho} = \left(-T_1 - \frac{g}{R}\right) \int_{z_0}^{z_1} \frac{dz}{T_0 + T_1 z} \qquad \text{(Section 2: -31)}$$

The integration is carried out using the following substitutions

$$\begin{aligned} u &= T_0 + T_1 z \\ du &= T_1 dz \\ dz &= \frac{du}{T_1} \end{aligned} \qquad \text{(Section 2: -32)}$$

giving

$$\int_{\rho_0}^{\rho_1} \frac{d\rho}{\rho} = \frac{\left(-T_1 - g/R\right)}{T_1} \int_{u_0}^{u_1} \frac{du}{u}. \qquad \text{(Section 2: -33)}$$

Integrating this expression gives

$$\ln \rho \Big|_{\rho_0}^{\rho} = -\left(1 + \tfrac{g}{RT_1}\right) \ln\left(T_0 + T_1 z\right)\Big|_{z_0}^{z} \qquad \text{(Section 2: -34)}$$

which when evaluated at the limits gives

$$\ln \rho - \ln \rho_0 = -\left(1 + \tfrac{g}{RT_1}\right)\left[\ln\left(T_0 + T_1 z\right) - \ln\left(T_0 + T_1 z_0\right)\right]. \qquad \text{(Section 2: -35)}$$

Solving for ln ρ gives the final expression

$$\ln \rho = \ln \rho_0 - \left(1 + \tfrac{g}{RT_1}\right) \ln\left(1 + \tfrac{T_1}{T_0}\left(z - z_0\right)\right). \qquad \text{(Section 2: -36)}$$

As was discussed in Section 2.1, this is a nonlinear least squares problem. This necessitates the use of the A matrix which is bound using the three parameters ln ρ_o, T_0, and T_1. Carrying out these partial derivatives give the following expressions

$$\frac{\partial \ln \rho}{\partial \ln \rho_0} = 1 \qquad \text{(Section 2: -37)}$$

$$\frac{\partial \ln \rho}{\partial T_0} = \frac{(RT_1 + g)T(z - z_0)}{RT_1T_0\left[T_0 + T_1(z - z_0)\right]} \qquad \text{(Section 2: -38)}$$

$$\frac{\partial \ln \rho}{\partial T_1} = -\frac{(RT_1 + g)(z - z_0)}{RT_1\left[T_0 + T_1(z - z_0)\right]} + \left[\ln\left(1 + \frac{T_1}{T_0}(z - z_0)\right)\right]\left(\frac{g}{RT_1^2}\right). \qquad \text{(Section 2: -39)}$$

The partial derivatives lead to an A matrix with size nx3, where n is the number of data points.

2.3.3 Bates Temperature Model

The Bates Temperature Model derivation is taken from the Keating, Nicholson, and Lake (1980) paper. The following form of the hydrostatic equation is used:

$$\frac{dn_i}{dz} + \frac{n_i}{T}\frac{dT}{dz} + \frac{n_i}{H_S} = 0 \qquad \text{(Section 2: -40)}$$

where H is the scale height and n_i is the number density of the i^{th} gas specie. Integrating this expression gives

$$n_{i,z} = n_{i,Zo}\left(\frac{T_{Zo}}{T_Z}\right)\exp\left(-\frac{m_i}{K}\int_{Zo}^{z} g(z)\frac{dz}{T}\right) \qquad \text{(Section 2: -41)}$$

where $g(z) = g_0(1 + z/R_m)^{-2}$, and g_0 is the acceleration of gravity at the effective surface of the planet. The temperature profile is given by

$$\begin{aligned} T(z) &= T_\infty - (T_\infty - T_{ZI})\exp\left[-s_1(z - z_I)\right], \quad z \geq z_I \\ T(z) &= T_L - (T_L - T_{ZI})\exp\left[s_2(z - z_I)\right], \quad z \leq z_I \end{aligned} \qquad \text{(Section 2: -42)}$$

which gives a temperature profile similar to Figure 2.3. Z_I is called the inflection point and occurs at the point where the two temperature sub-profiles have the same slope. The inflection point is labeled by a point in Figure 2.3.

Walker (1965) showed that a closed form solution to the hydrostatic equation can be found by substituting $-\sigma\beta$ for the terms $s_x(z-z_0)$, where

$$\sigma = s + \frac{1}{R + z_0} \qquad \text{(Section 2: -43)}$$

and

$$\beta = \frac{(z - z_0)(R + z_0)}{R + z} \qquad \text{(Section 2: -44)}$$

(2.beta)

with (2-44) being the geopotential altitude. This leads to the solution of the hydrostatic equation for $z \geq z_l$

$$n_{i,Z} = n_{i,Zi}\left(\frac{T_{Zi}}{T_Z}\right)^{1+\gamma_i} \exp\left(-\sigma\gamma_i\beta\right) \qquad z \geq z_I \qquad \text{(Section 2: -45)}$$

where

$$\gamma_i = \frac{m_i g_{Z_I}}{\sigma K T_\infty} \qquad \beta = \frac{(z - z_I)(R_m + z_I)}{R_m + z} \qquad \text{(Section 2: -46)}$$

and for $z \leq z_l$,

$$n_{i,Z} = n_{i,Zi}\left(\frac{T_{Zi}}{T_Z}\right)^{1+\gamma_i'} \exp\left(-\sigma\gamma_i'\beta\right) \qquad z \geq z_I \qquad \text{(Section 2: -47)}$$

where,

$$\gamma_i' = \frac{m_i g_{Z_I}}{\sigma K T_L}. \qquad \text{(Section 2: -48)}$$

The density, ρ, as a function of altitude is found by the expression

$$\rho(z) = \sum_i n_i m_i \qquad \text{(Section 2: -49)}$$

where i is the number of constituents considered. For these models three major constituents are assumed: CO_2 (molecular weight 44), O_2 (molecular weight 16), and a combination of N_2 and CO (molecular weight 28). Also, since number densities are used to generate the overall density profile, it is necessary to assume mixing ratios for the three different constituents. As in all non-linear least square models, it is necessary to have a first guess for the model parameters. The base density is assumed and then the mixing ratios are used to find the initial estimate for each constituent's base number density. For these models, the mixing ratios at 125 km are assumed to be 95% CO_2, 3% N_2+CO, and 2% O. The mean molecular weight for the atmosphere can also be found from the mixing ratios using the following expression

$$M_{atm} = M_{CO_2}(\%CO_2) + M_{N_2+CO}(\%N_2 + CO) + M_O(\%O) \qquad \text{(Section 2: -50)}$$

For this model, there are five fit parameters, T_∞, T_L, s_1, s_2, ρ_0, and T_{zl}. Again, the partial derivatives with respect to each of these parameters must be found. Due to the complexity of this model, a finite difference method is used to find the partial derivatives instead of finding analytic partial derivatives. This is done as shown in (2-51), which is a central difference partial for the parameter T_∞.

$$\frac{\partial n_{i,z}}{\partial T_\infty} = \frac{n_{i,z}(T_\infty + \Delta T_\infty) - n_{i,z}(T_\infty - \Delta T_\infty)}{2\Delta T_\infty} \qquad \text{(Section 2: -51)}$$

This technique is also used to find partial derivatives for the other four parameters.

2.3.4 Latitudinal Variation Model

The latitudinal variation model is created by adding another term to the least squares model. This latitudinal variation term has the form

$$LV = \alpha(L - L_0) \qquad \text{(Section 2: -52)}$$

where α is the strength of the latitudinal variation in units of percent variation per degree of latitude. L is a range of latitudes throughout the aerobraking pass, and L_0 is a reference latitude. Recall, the constant temperature model is

$$\ln\rho = \ln\rho_0 - \frac{g}{RT}(z - z_0) \qquad \text{(Section 2: -53)}$$

The only difference between the latitudinal variation model and the constant temperature model is the addition of the term (2-52) resulting in the expression

$$\ln\rho = \alpha\left(lat - lat_0\right) + \ln\rho_0 - \frac{g}{RT}\left(z - z_0\right) \qquad \text{(Section 2: -54)}$$

The added term in this model adds another fit parameter, α, to the fit. Again, we must find the A matrix for this model. The A matrix is the same as that of the constant temperature model except for an added column due to the added term, α. This partial has the form

$$\frac{\partial \ln\rho}{\partial \alpha} = \left(L - L_0\right). \qquad \text{(Section 2: -55)}$$

2.4 Additional Information From The Models

All of the least squares fits discussed above are density fits. Therefore, a fit will give an empirical density model. However, more information can be found from the modeled data. This additional information comes from the fit parameters and relationships between density and other values such as pressure.

For each of the models, a temperature profile was assumed, and is described in some way by the fit parameters. For example, in the constant temperature model, the temperature profile is found indirectly since the parameters are ρ_0 and scale height, H_s. From scale height, we find the temperature using the relationship

$$H_s = \frac{kT}{mg} \qquad \text{(Section 2: -56)}$$

In the linear temperature model, the fit parameters are ρ_0, T_0, and T1. The temperature is found by a combination of these parameters in the form

$$T = T_0 + T_1 z \qquad \text{(Section 2: -57)}$$

The same can be done for both the Bates model and the latitudinal variation models, giving a temperature vertical structure over the given range of altitudes.

Pressure is found using the density profile and the temperature profile by the relationship

$$p = \rho RT \qquad \text{(Section 2: -58)}$$

By comparing the generated model to the actual data, a set of residuals (ε_i) can be generated as shown in (2-3) and (2-4). The residuals give more information about the quality of the fit to the data set. In an ideal fit, the residuals look like white noise. This tells that the model accurately represents the data and that all error comes from the measurement errors in the instrument. However, it is difficult to fully model a real world system because It is impossible to foresee all the essential parameters. This is

especially the case with modeling the Martian atmosphere of which so little is known. When all the necessary parameters are not included in the model, trends arise in the residuals. These trends can be seen visually and are numerically quantified by the standard deviation. The residuals are easily calculated in log 10 space by

$$\varepsilon_i = y_{oi} - y_{ci} = \log_{10}\rho - \log_{10}\hat{\rho} \qquad \text{(Section 2: -59)}$$

where ρ is the calculated density profile. The standard deviation of a sample population can then be calculated from the expression

$$\sigma = \sqrt{\frac{\sum_{i=1}^{n}(E_n)^2}{n-1}} \qquad \text{(Section 2: -60)}$$

The standard deviation tells the accuracy of the overall data fit.

It is also possible to find the error on each of the model parameters by finding the covariance matrix. This is easily done using the expression

$$\Gamma_x = \sigma^2\left(A^T A\right)^{-1} \qquad \text{(Section 2: -61)}$$

For the linear temperature profile, this would result in the following

$$\Gamma_x = \begin{bmatrix} \sigma^2_{\ln\rho_0} & \rho_{12} & \rho_{13} \\ \rho_{22} & \sigma^2_{T_0} & \rho_{22} \\ \rho_{13} & \rho_{12} & \sigma^2_{T_1} \end{bmatrix}, \qquad \text{(Section 2: -62)}$$

where the σ's represents the error on each parameter and the ρ's represent the correlation between the parameters. So, taking the square root of the diagonal of Γ_x gives the errors on the individual parameters and can be used to determine the accuracy of the least squares solution for the different parameters.

Section 3: Results

3.1 Fit to Known Vertical Structures

Once the models were created, they were applied to known vertical structures to test their accuracy and robustness. The three vertical structures used came from planetary landers Viking I (20 July 1976), Viking II (3 September 1976), and Pathfinder (4 July 1997). Figure 3.1 shows fits of density data from both Viking landers assuming a constant temperature profile.

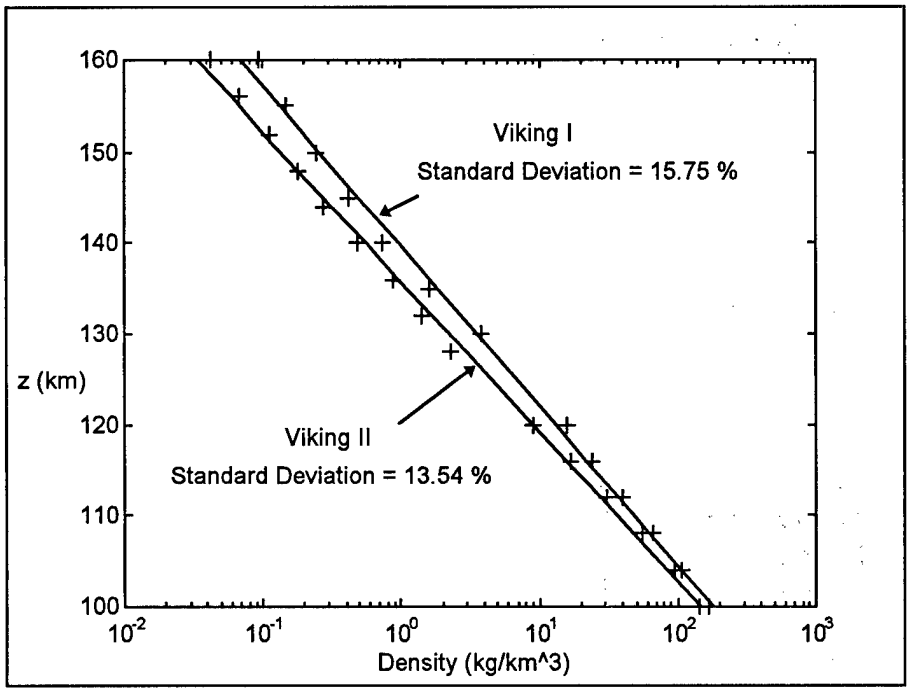

Figure Section 3: .1: Least Squares Fit to Viking Entry Data (Constant Temperature Profile)

Figure 3.2 shows fits of density data from the same landers, except assumes a linear temperature profile. Note that the standard deviations from the linear temperature fit are lower in both cases. However, the constant temperature model does an accurate job at modeling the atmosphere in both cases.

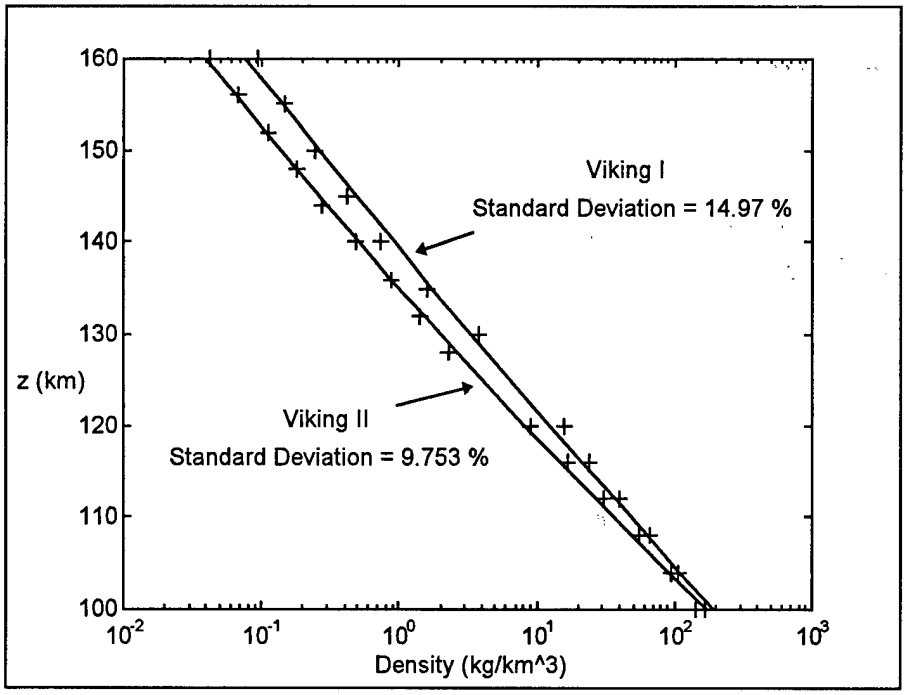

Figure Section 3: .2: Least Squares Fit to Viking Entry Data (Linear

Figures 3.3-3.5 show fits to the Pathfinder density data assuming the three different temperature profiles.

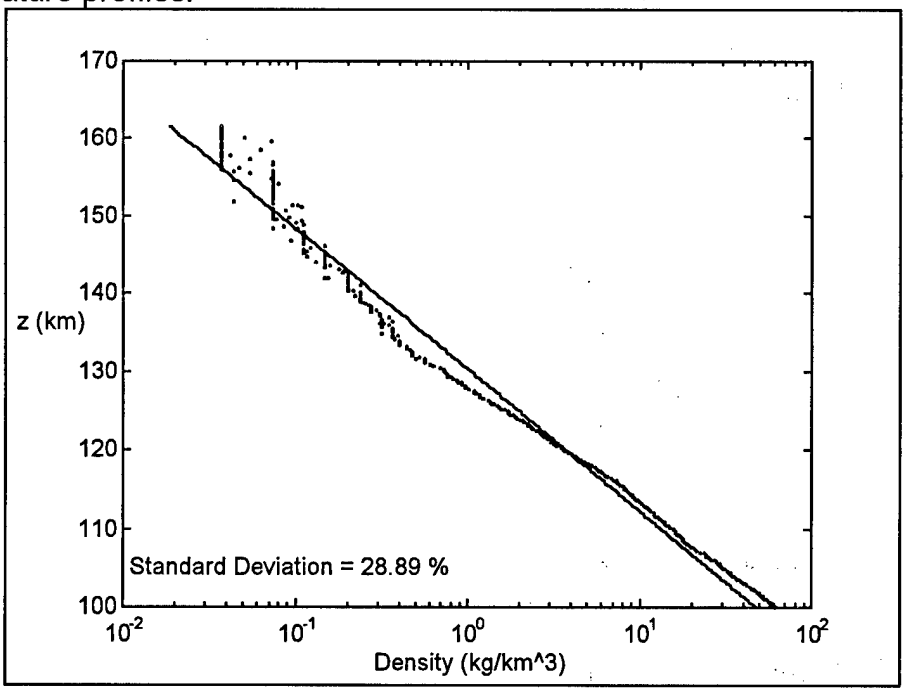

Figure Section 3: .3: Least Squares Fit to Pathfinder Entry Data (Constant Temperature Profile)

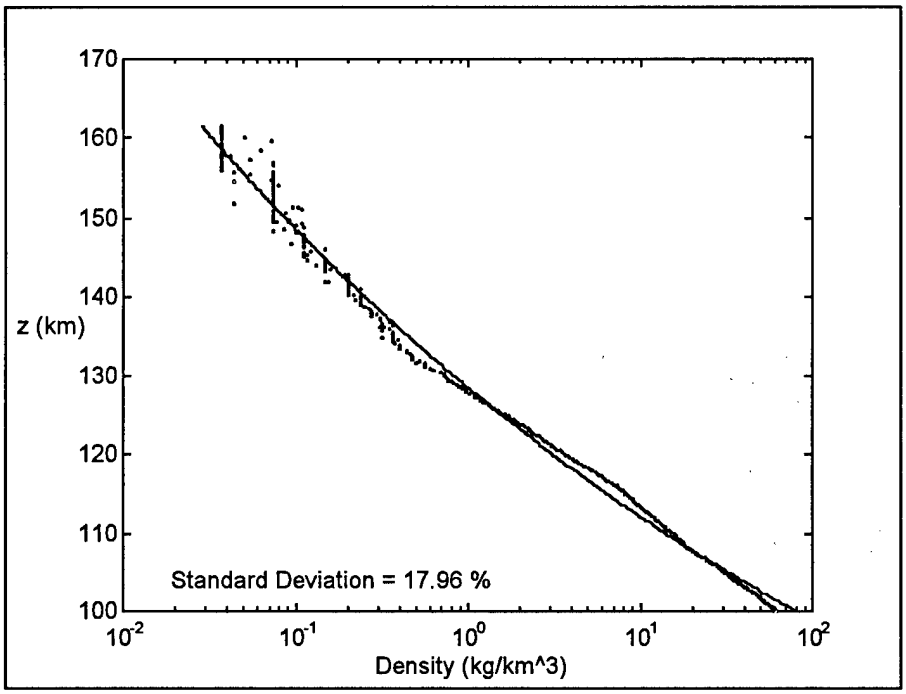

Figure Section 3: .4: Least Squares Fit to Pathfinder Entry Data (Linear Temperature Profile)

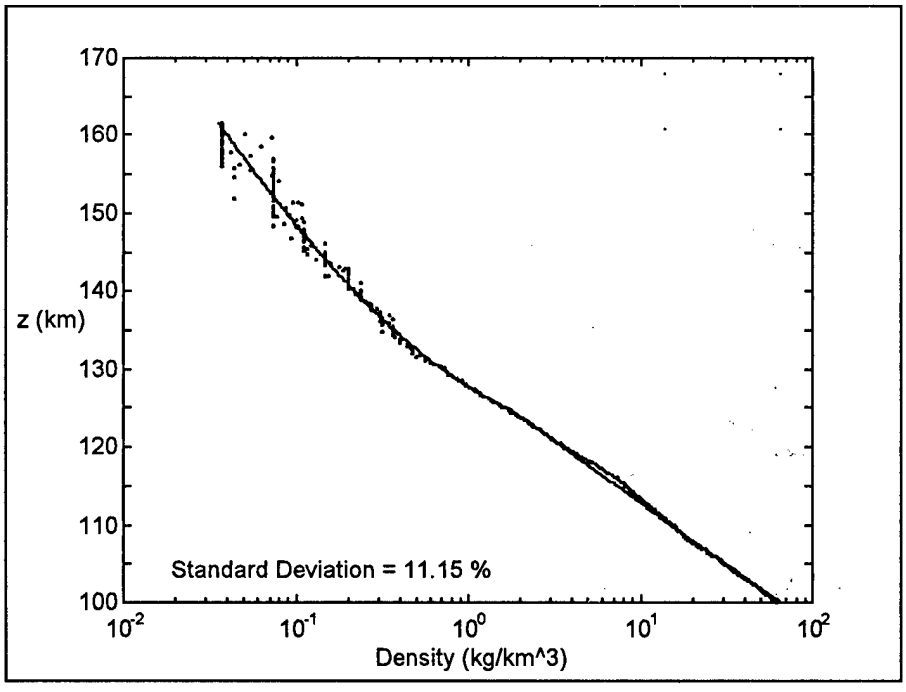

Figure Section 3: .5: Least Squares Fit to Pathfinder Entry Data (Bates Temperature Profile)

Table 3.1 summarizes the fit quality of the different models judged by the standard deviation of the fit.

Lander	Constant Temp.	Linear Temp.	Bates Temp.
Viking I	15.75%	14.97%	N/A
Viking II	13.54%	9.75%	N/A
Pathfinder	28.89%	17.96%	11.15%

Table Section 3: -1: Standard Deviations of Fits To Various Lander Density Vertical Structures

For each lander, it is seen that the fit quality is better as the complexity of the model increases. This is expected due to the fact that least squares models usually become more accurate when extra parameters are introduced. This is the case with the three models compared here. The constant temperature model has two terms, the linear temperature model has three, and the Bates temperature model has five. Notice that the complex Bates model doesn't converge to a solution for the two Viking cases. Due to the complexity of the model, the atmosphere must exhibit certain precise characteristics in order to obtain convergence. It was found that the Bates model either would not converge, or would converge to an inaccurate temperature result if the atmosphere was nearly isothermal. Therefore, seeing that the two Viking landers experienced nearly isothermal atmospheres, it is not surprising that the Bates model did not converge to a solution for these two cases.

These results gave confidence that the chosen least squares models, that they would be able to accurately model the atmosphere MGS encountered as it began its aerobraking mission.

3.2 Fit to MTGCM Model

The next step in evaluating the validity of the models was to compare them to an existing Martian atmospheric model. Specifically, the least squares models were compared to the MTGCM model developed by Steve Bougher of the University of Arizona. The MTGCM model gave a density vertical structure with corresponding temperatures. The least squares models were evaluated by using the density vertical structure as the test data. The fit quality could then be evaluated, and the resulting least squares temperature profile could be compared with the MTGCM temperature profile. Figures 3.6-3.8 show the different fits to the MTGCM density data for a case in January 1998.

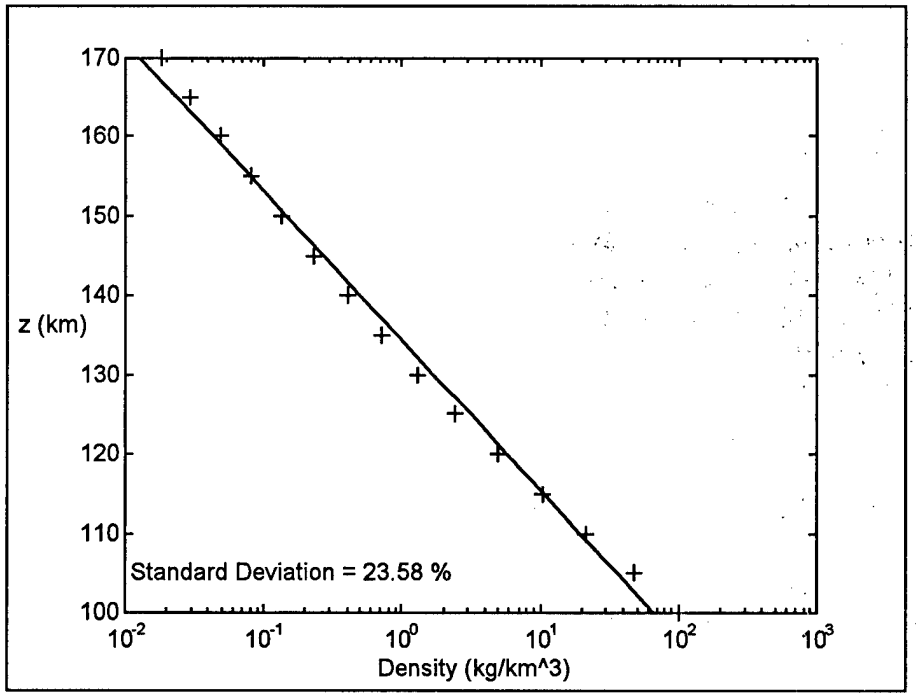

Figure Section 3: .6: Least Squares Fit to MTGCM Model Assuming a Constant Temperature Profile

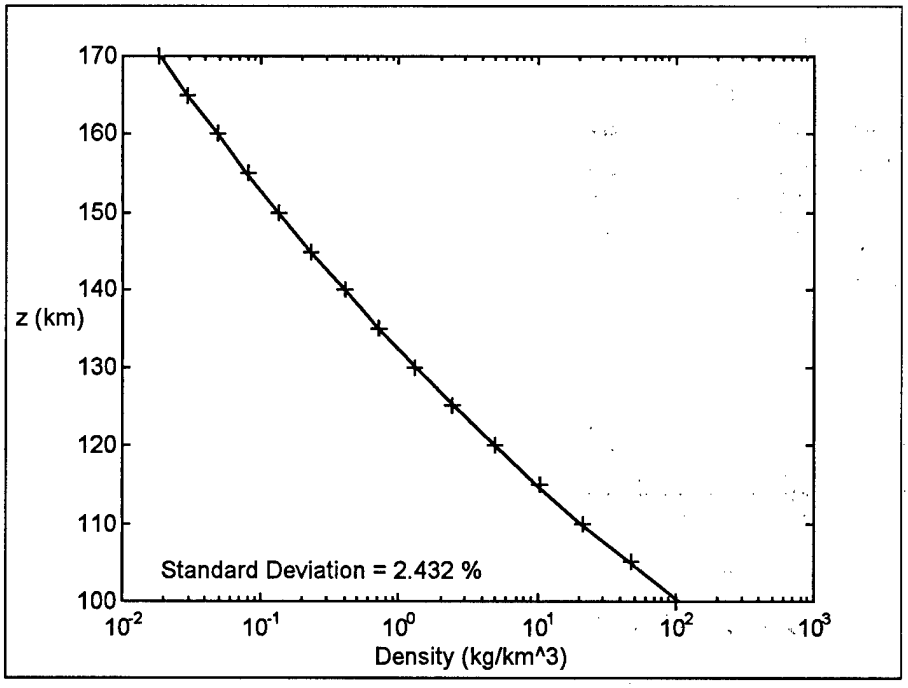

Figure Section 3: .7: Least Squares Fit to MTGCM Model Assuming a Linear Temperature Profile

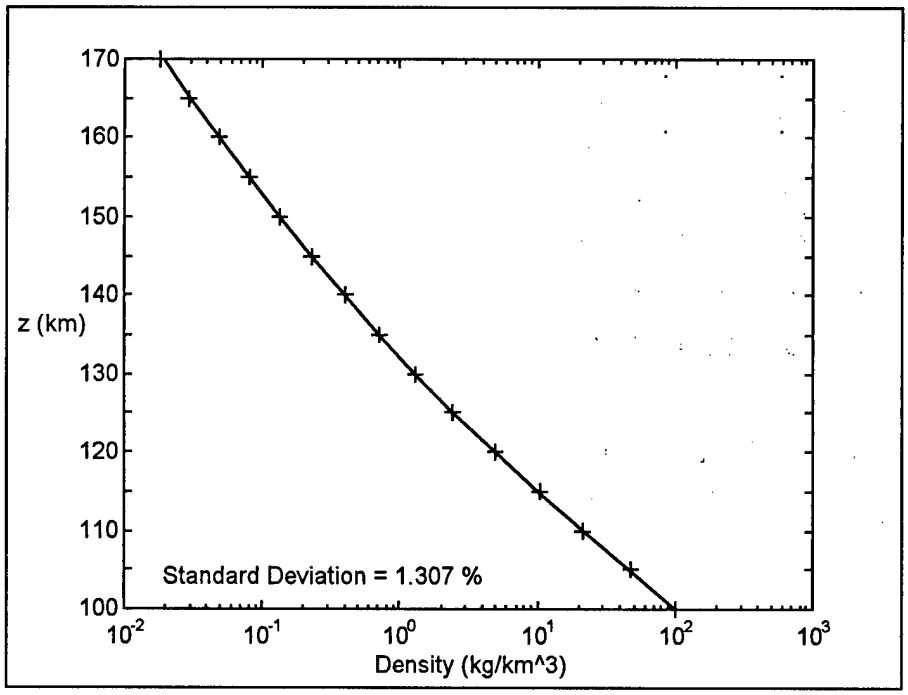

Figure Section 3: .8: Least Squares Fit to MTGCM Model Assuming a Bates Temperature Profile

Again, it is seen that the fit quality increases by using the more complex models. Notice in Figure 3.8 that nearly a perfect fit was achieved with a standard deviation of 1.31%.

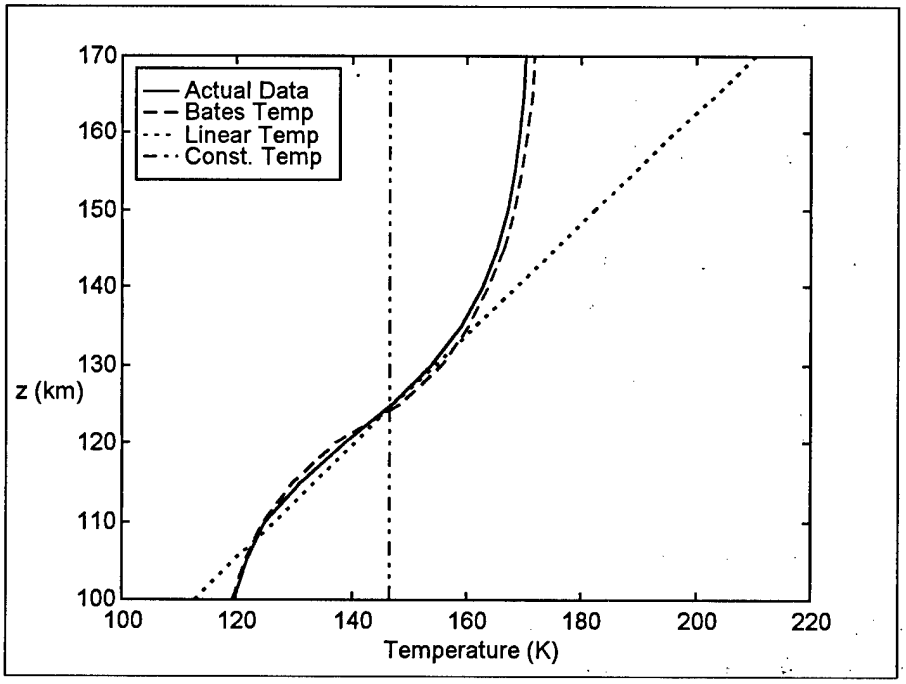

Figure Section 3: .9: Temperature Profile Comparison for Fits to MTGCM Model

Figure 3.9 shows a comparison of the MTGCM temperature profile and the temperature profiles from the least squares fits. Again, the Bates temperature profile is almost a perfect fit to the MTGCM model. This explains why the density fit seen in Figure 3.8 is so accurate. At first glance, it seems that the constant and linear temperature profiles do not represent the "actual" temperature profile very well. However, upon closer investigation, it is seen that these two models do give fairly accurate temperatures at lower altitudes, and especially around 125 km. Considering that aerobraking altitudes are around 100-140 km, all three models give temperatures that are fairly close to the "actual" temperature.

A factor to consider is that the MTGCM data is perfect data. As a model, there are no data gaps or factors decreasing the quality of the data. This means that even the complex models will return results when fit to the data. However, the true spacecraft data is not this perfect. Various factors ranging from data errors (bias, digitization, etc.) to spacecraft vibrations picked up by the accelerometers cause imperfections in the data. These data imperfections will be discussed further in Section 3.3. Imperfect data can make convergence difficult for the more complex models. This makes the simple constant temperature model even more important. With the constant temperature model giving accurate density and temperature profiles, it is possible to understand the Martian atmosphere, even with imperfect data.

3.3 Actual Data

As expected, the accelerometer data received wasn't perfect. On early orbits, one full second of accelerometer data was received for every eight seconds of real time. With this limited amount of data, there was significant digitization error at higher altitudes. This is seen in Figure 3.10 for Periapsis 12.

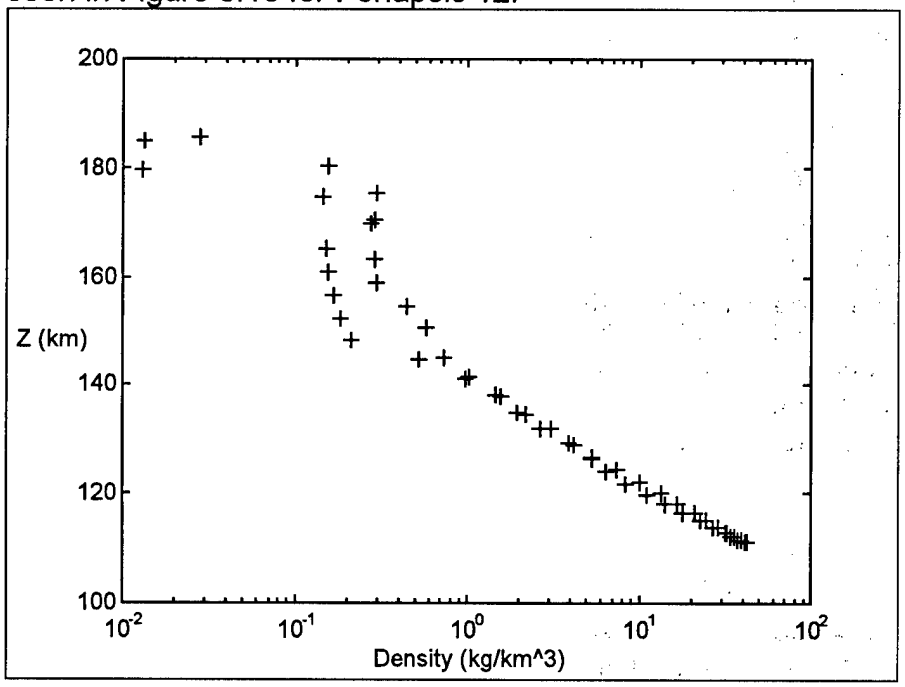

Figure Section 3: .10: P012 Averaged Accelerometer Data

Although the accelerometers recorded data up to around 185 km, only data up to about 140 km could be considered reliable. This meant that there was about 30 km of usable data. It turned out that this was not enough data to generate accurate models using the more complicated linear and Bates models. However, the constant temperature model did give accurate and reliable data which corresponded with results generated by the spacecraft navigation team.

It was often apparent that there was a temperature change in the atmosphere (corresponding to a curve in the density vs. altitude plots) over the 30 km of valid data. Therefore, it was unreasonable to assume that the constant temperature profile gave accurate temperature data over that entire range. Considering this situation, it was necessary to develop a technique that could use the robust constant temperature model to describe the entire altitude range, or at least specific areas of interest. The technique used to do this involved looking at a specific region of interest. For example, to find the temperature at 130 km, data from 120-140 km would be modeled. This would give a more accurate temperature reading at 130 km. The same could be done for any altitude of interest.

Later in the mission, the accelerometer data was returned at one full second every second. This, in effect, produced eight times the amount of data as on early orbits and allowed for more complex modeling. An example of this additional data is shown in Figure 3.11 for Periapsis 68.

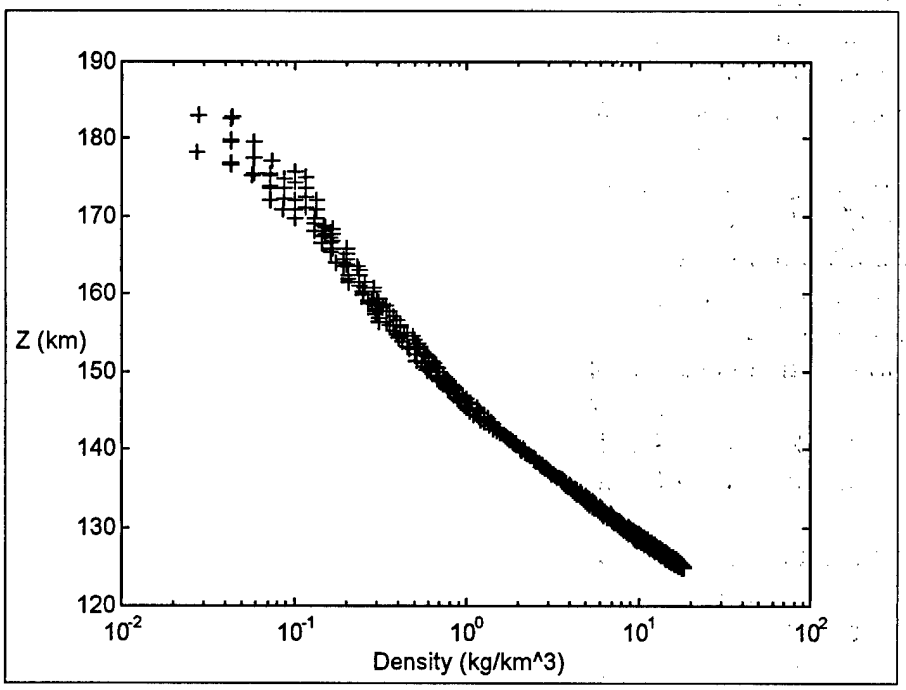

Figure Section 3: .11: P068 Averaged Accelerometer Data

Notice that there are more data points for a periapsis pass and that the range of valid data goes up to about 170 km. With this added data, it was possible to use the linear and Bates temperature models to model the atmosphere.

However, in some cases, it was still not possible to use these models. An example of this situation occurred for Periapsis 65 as seen in Figure 3.12.

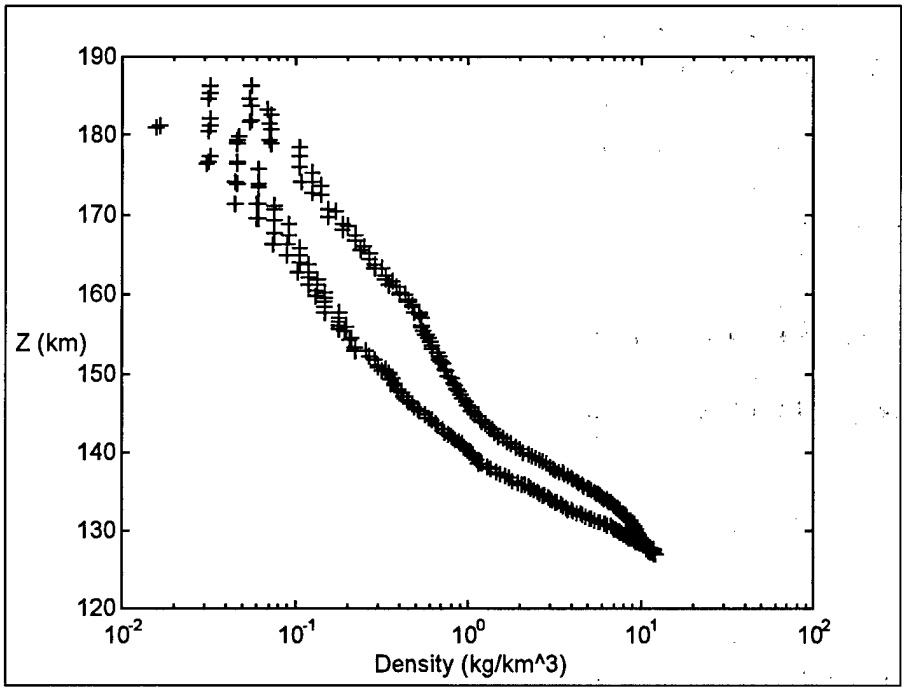

Figure Section 3: .12: P065 Averaged Accelerometer Data

The latitudinal variation and the digitization error make it impossible to model the atmosphere with anything other than with a constant temperature model over specific regions of interest.

3.4 Analyzing the MGS Accelerometer Data

In this section, the MGS accelerometer data will be analyzed. The different temperature models will be looked at for nominal situations and then an atmospheric disturbance will be discussed.

3.4.1 Fits of the Various Models

The least squares models were effective in characterizing the atmosphere encountered by MGS on it's aerobraking passes. Figures 3.13-3.15 show fits of the various models to data from Periapsis 043.

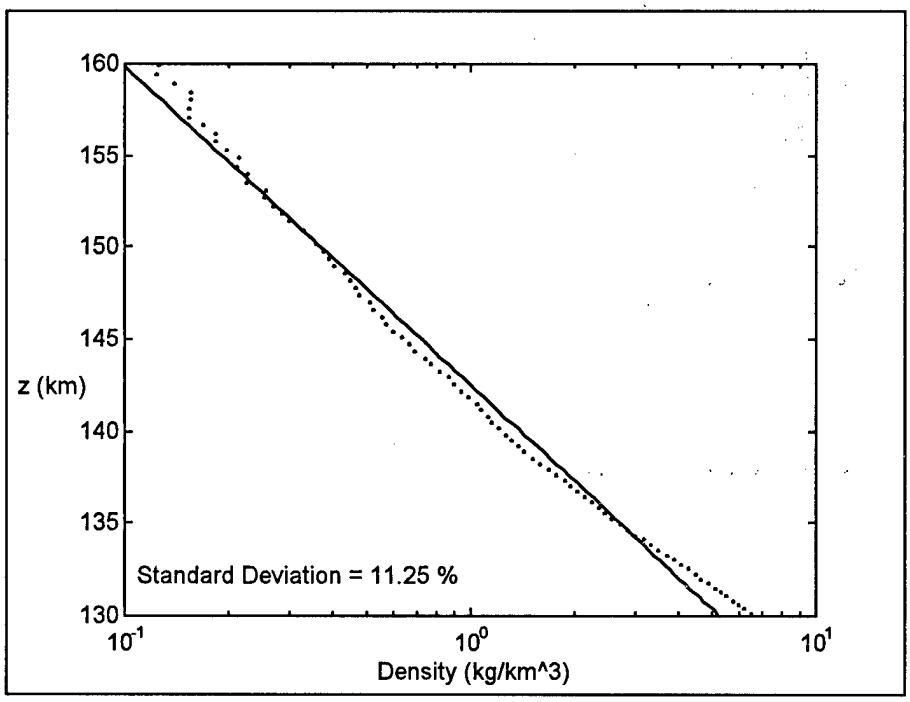

Figure Section 3: .13: Least Squares Fit to Periapsis 43 Data (Constant Temperature Profile)

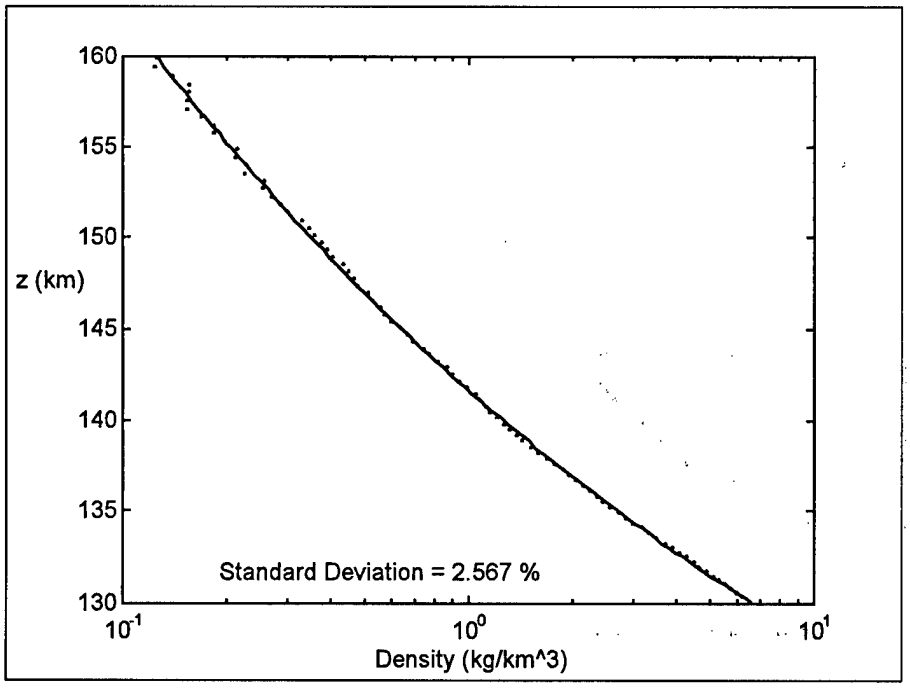

Figure Section 3: .14: Least Squares Fit to Periapsis 43 Data (Linear Temperature Profile)

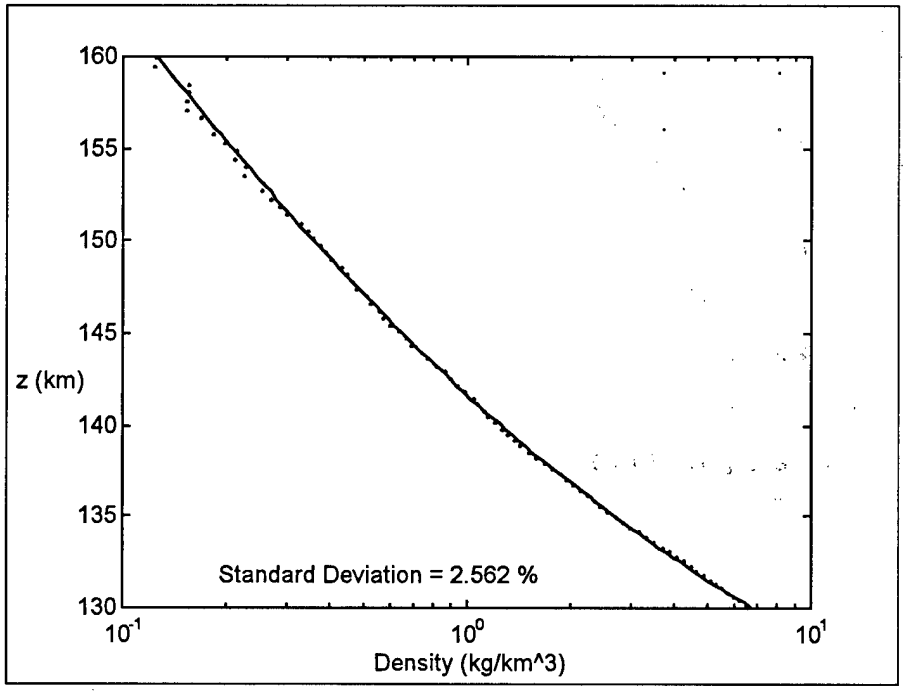

Figure Section 3: .15: Least Squares Fit to Periapsis 43 Data (Bates Temperature Profile)

For this periapsis, data was used from 130-160 km and all of the models converged to a solution. Looking at the standard deviations of the three models, the increased fit quality of the more complex models is seen with the standard deviation going from 11.25% for the constant temperature model to around 2.56% for both the linear and Bates temperature models. There is a slight increase in fit quality of the Bates temperature model over the linear temperature model as well. This seems to indicate that these two models give similar results, however, there are significant differences in the corresponding temperature profiles. A comparison of the different temperature profiles is shown in Figure 3.16.

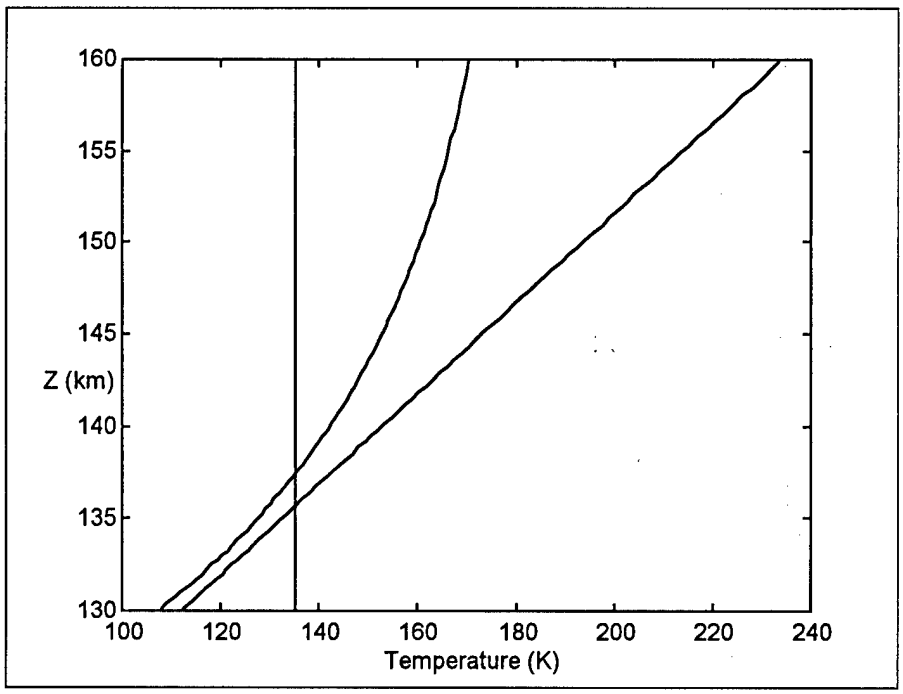

Figure Section 3: .16: Temperature Profiles for Periapsis 43 (Constant, Linear, and Bates Profiles)

Again, all of the models give similar temperatures around 135 km. But, looking at the exospheric temperatures, there is a large difference between the linear and Bates profile. Experience tells that the large temperatures given by the linear temperature model at high altitudes are unrealistic. Traditionally, atmospheric temperature structures are described by models similar to the Bates profile. Therefore, it is seen that at lower altitudes, the most crucial part of the periapsis pass, the linear temperature model gives accurate results. However, it is necessary to use the Bates model to characterize temperatures at the higher altitudes.

3.4.2 Characterization of an Atmospheric Disturbance

As an example of the effectiveness and necessity of modeling the accelerometer data from the MGS aerobraking passes, plots of several successive orbits will be shown to depict an atmospheric disturbance that endangered the spacecraft. This is seen in Figures 3.17-3.20. The first plot is the constant temperature least squares fit to Periapsis 12. For this orbit, the periapsis density was about 37.5 kg/km^3.

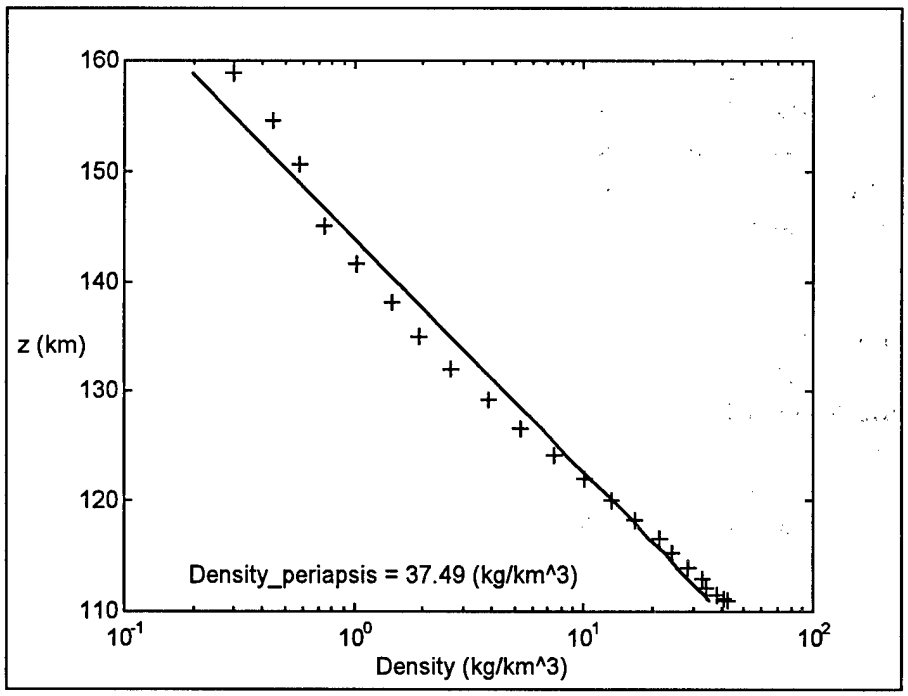

Figure Section 3: .17: Fit to Outbound Leg of Periapsis 12

The periapsis density for Periapsis 13 was about 55 kg/km^3 and for Periapsis 14 was about 56 kg/km^3.

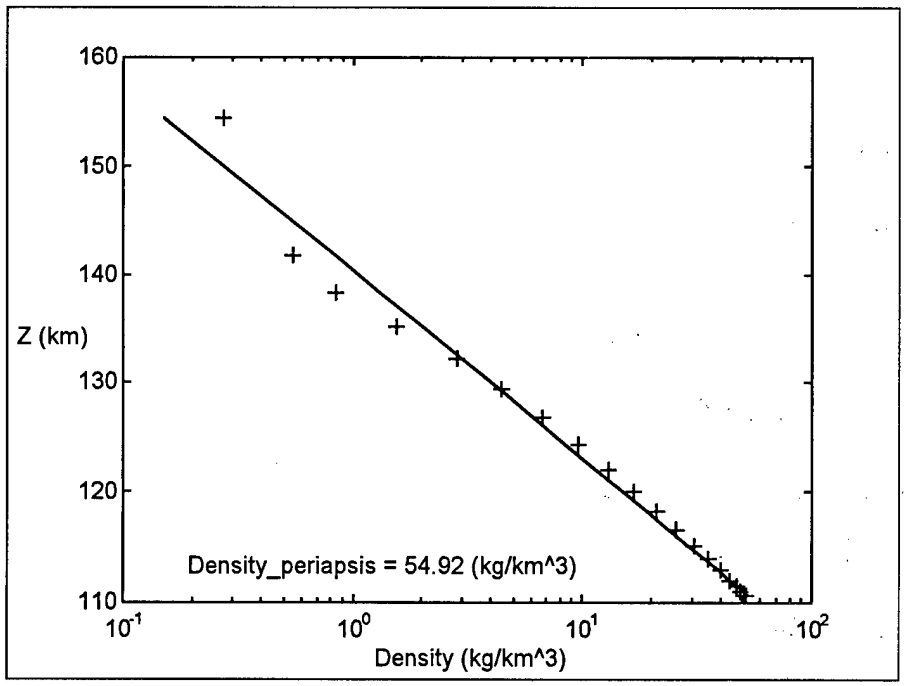

Figure Section 3: .18: Fit to Outbound Leg of Periapsis 13

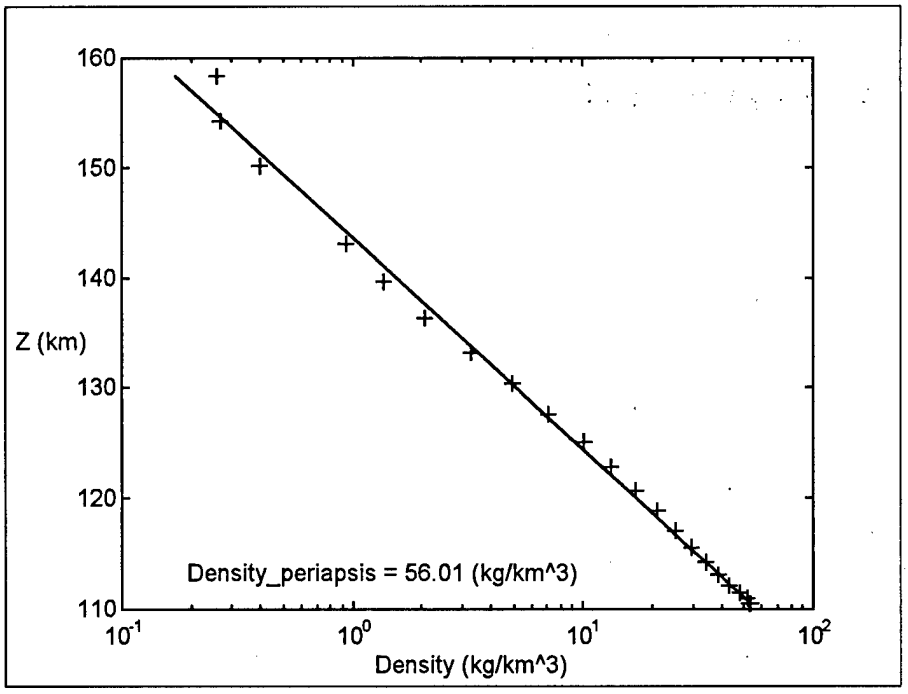

Figure Section 3: .19: Fit to Outbound Leg of Periapsis 14

Then, on Periapsis 15, the periapsis density jumped to about 82.5 kg/km^3.

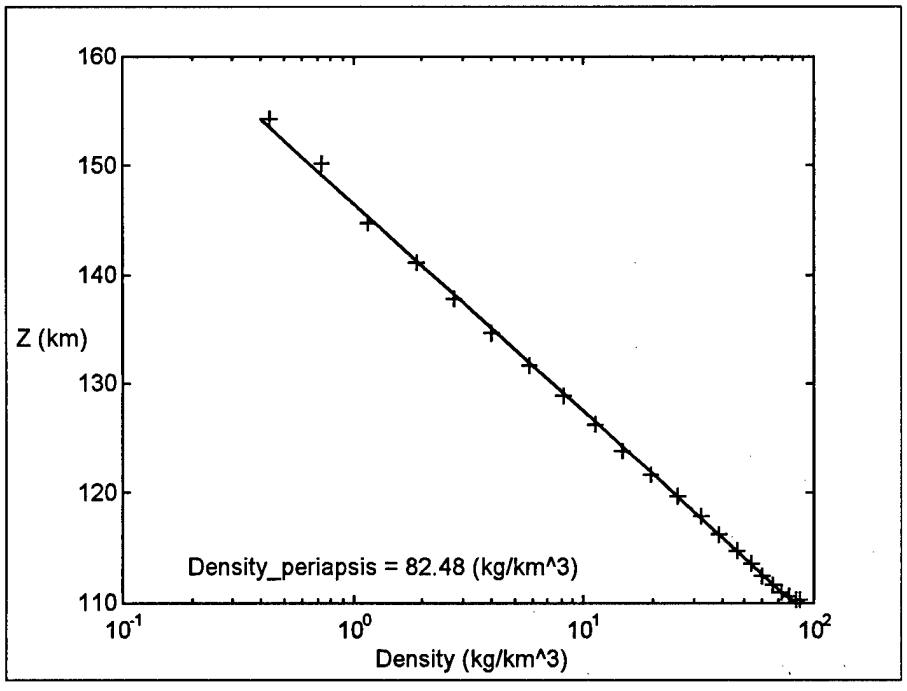

Figure Section 3: .20: Fit to Outbound Leg of Periapsis 15

This large density increase caused the dynamic pressure to move outside the safe corridor for the spacecraft and caused structural damage to one of the solar arrays. For

Periapsis 16, the spacecraft's periapsis was raised about 10 km due to the large density increase on Periapsis 15. Figure 3.21 shows a fit to the combined inbound and outbound legs of Periapsis 16.

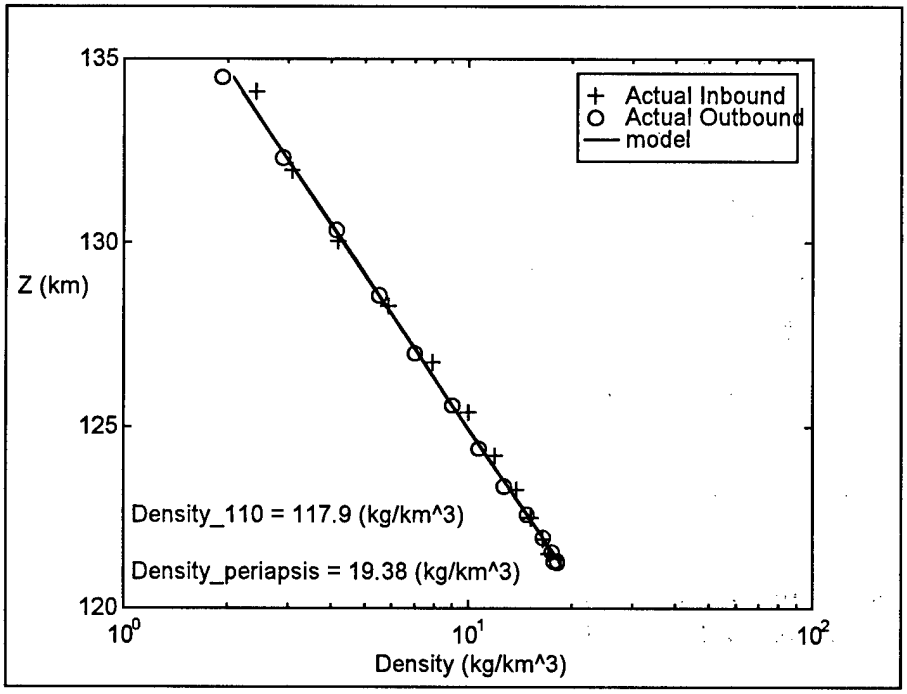

Figure Section 3: .21: Fit to Periapsis 16

Extrapolating the Periapsis 16 model down to 110 km showed that the density could have been around 115 kg/km^3 if the periapsis altitude had remained near 110 km. This could have caused more damage to the spacecraft had the density increase not been quickly noticed. This situation showed the importance of atmospheric modeling using the accelerometer data and demonstrated the need for constant monitoring of the poorly known atmosphere. The damage to the solar array caused a several week aerobraking hiatus and significantly affected further aerobraking scheduling. The atmospheric disturbance could have resulted in mission loss if it hadn't been quickly and accurately measured.

3.5 Analysis of the Least Squares Residuals

As discussed in the Theory section, the residuals of the least squares fits can be generated to show trends in data sets and measure the quality of the fit. Again, for a perfect fit, the residuals will look like white noise, signifying that all necessary parameters are included in the least squares fit. Figure 3.22 shows a set of residuals from a fairly accurate fit. These residuals come from the Bates temperature model fit of the MGTCM model. Although the fit is not perfect, it gives an idea of what the residuals will look like for an accurate fit.

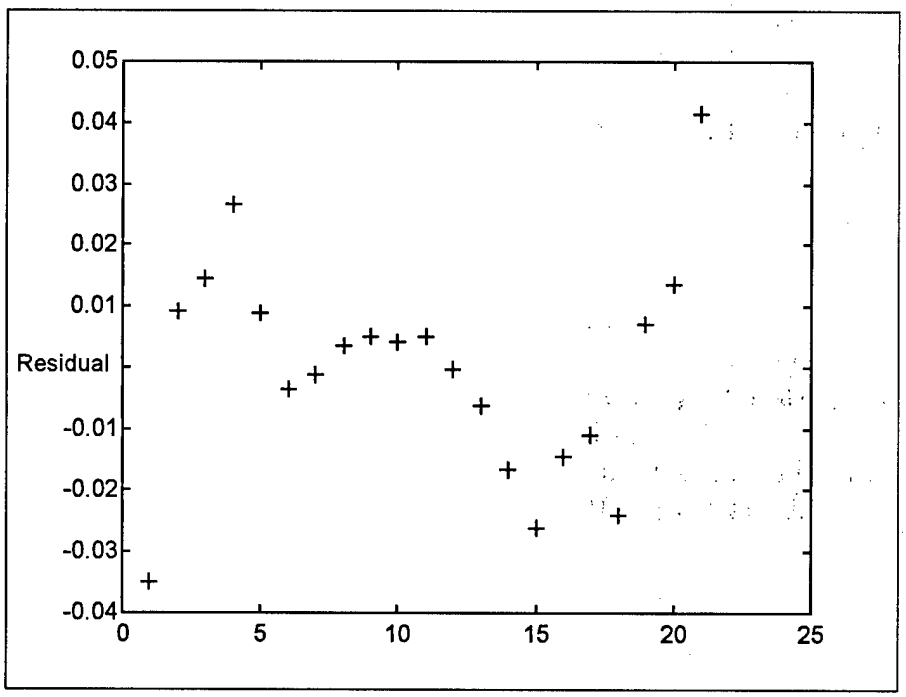

Figure Section 3: .22: Example of Residuals for Fit to MGTCM Model (Bates Temperature Profile)

3.5.1 Latitudinal Variation

In analyzing the MGS accelerometer data, there were often missing parameters in the models that disallowed accurate characterization of the Martian atmosphere. The biggest trend that was seen came from a latitudinal variation in the atmosphere. This caused large differences in the inbound and outbound leg of the periapsis pass which is clearly seen on Periapsis 14 from 110 km up to about 140 km in Figure 3.23.

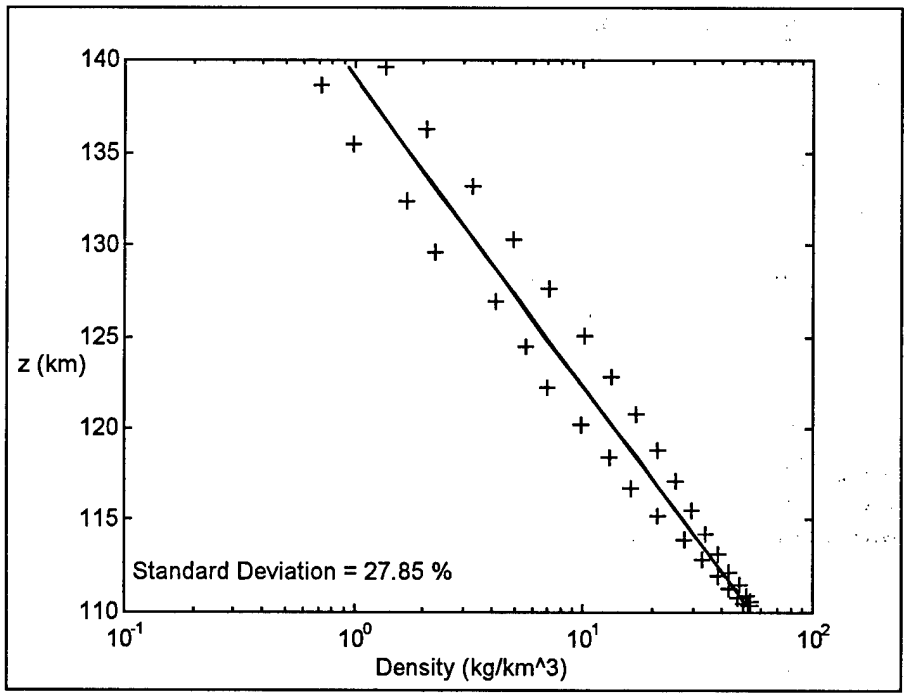

Figure Section 3: .23: Least Squares Fit to Periapsis 014 Data (Constant Temperature Profile)

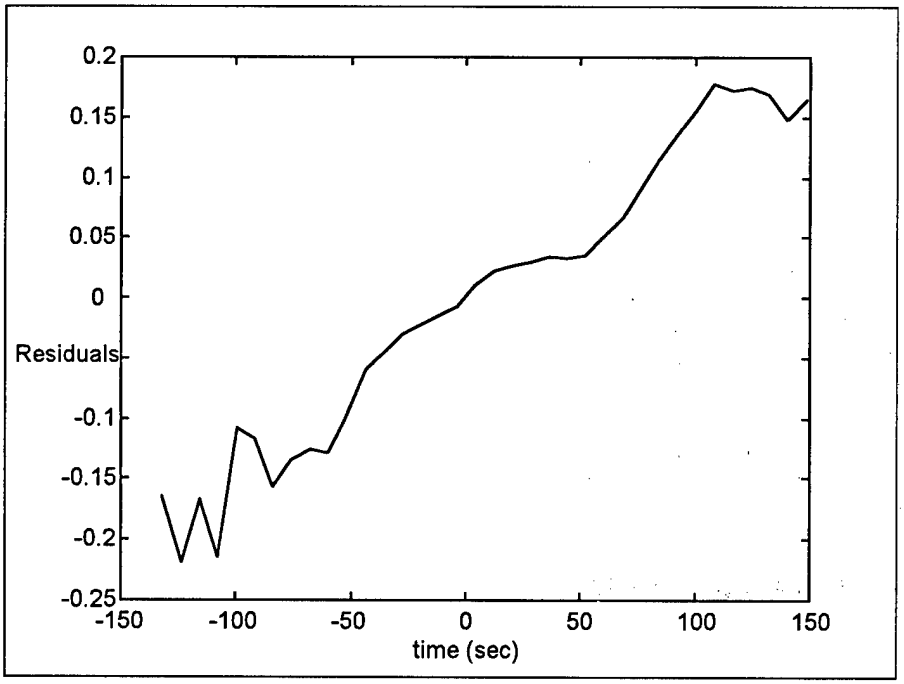

Figure Section 3: .24: Residuals For Fit of Periapsis 014 Data (Constant Temperature Profile)

The upward trend of the residuals, shown in Figure 3.24, shows the shortfall of this model. The constant temperature model fits the data with a line in between the inbound and outbound leg, inaccurately modeling both legs. One way to generate accurate models for both legs is to separate the data into inbound and outbound legs and model them separately. However, this neglects the latitudinal variation, an important characteristic of the atmosphere. It became apparent in the Martian atmosphere that the latitudinal variation was key to predicting large atmospheric disturbances that could endanger the spacecraft. Therefore, it was necessary to quantify the latitudinal variation. This was done as shown in Section 2.4.4. With an extra parameter in the model, the result is shown in Figure 3.25.

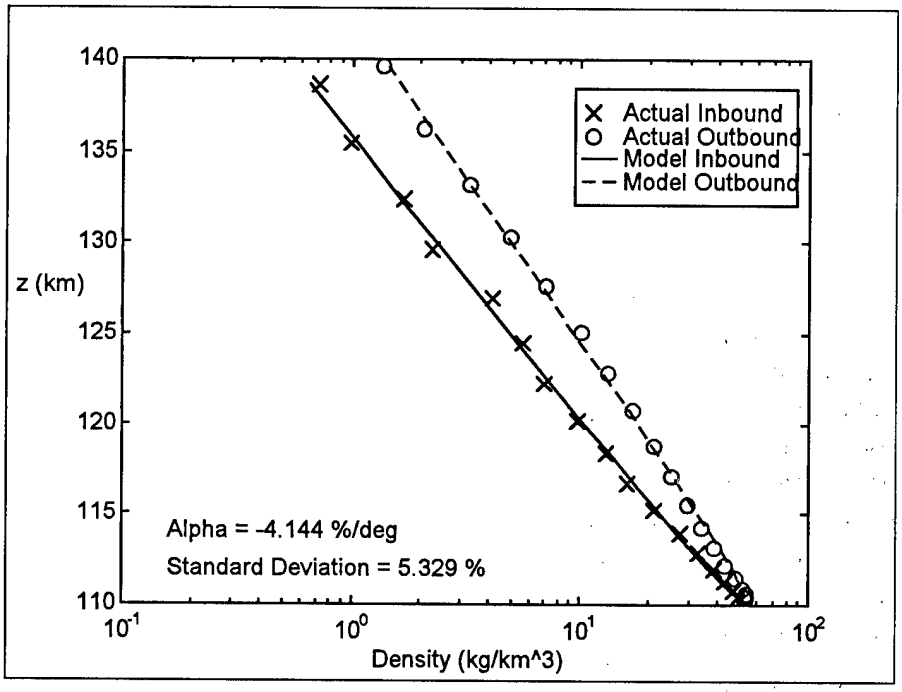

Figure Section 3: .25: Least Squares Fit to Periapsis 014 Data (Latitudinal Variation with Constant Temp Profile)

The model now follows both the inbound and outbound leg. The residuals in Figure 3.26 show that the fit is much better and the decrease in standard deviation from 27.85% to 5.33% quantifies this improvement.

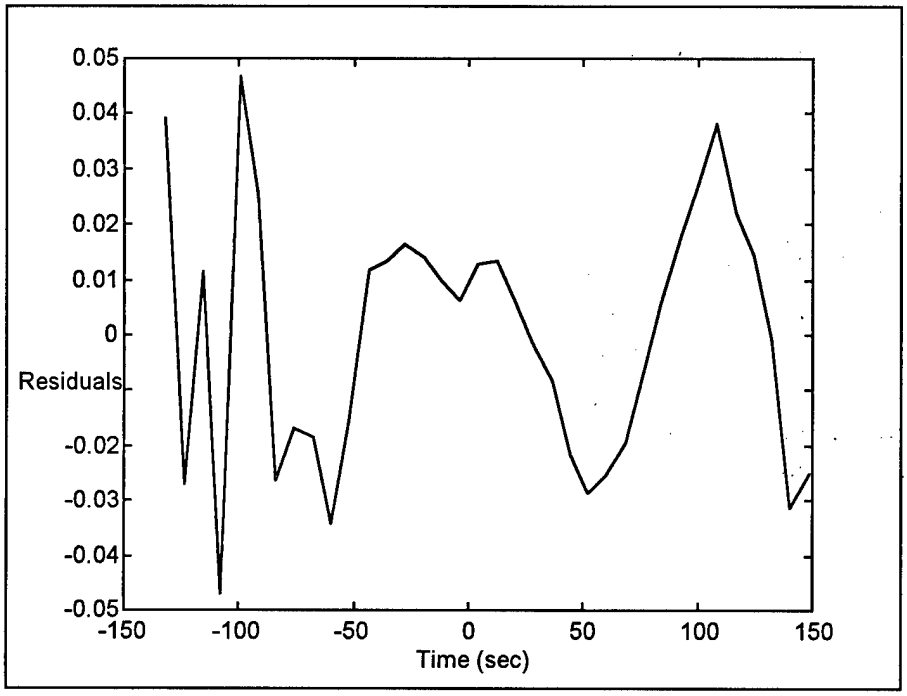

Figure Section 3: .26: Residuals For Fit of P014 Data (Latitudinal Variation With Constant Temperature)

3.5.2 Wave Activity

Wave activity is another phenomenon that is shown by the residuals. Figure 3.27 shows the inbound leg of Periapsis 56.

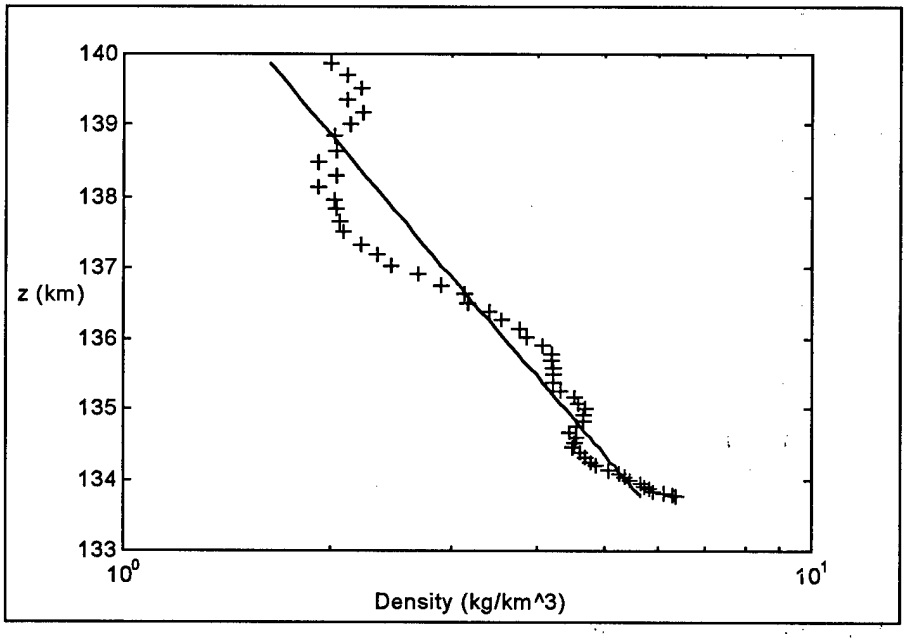

Figure Section 3: .27: Wave Activity on Inbound Leg of

It is evident that the constant temperature model fits the data trend but does not accurately model the fine details. The residuals in Figure 3.28 show the fine wave activity in the atmosphere.

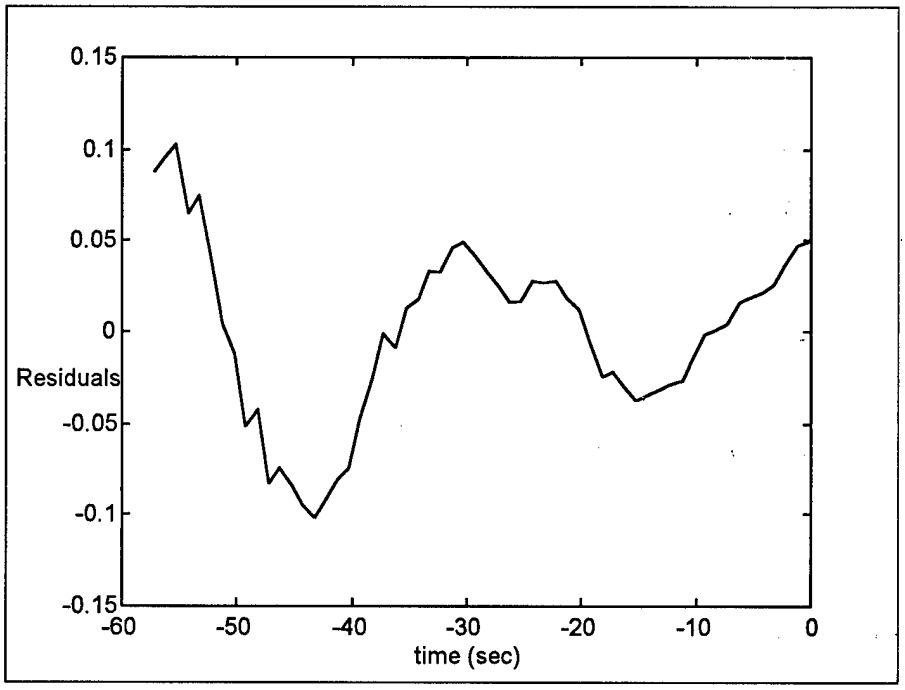

Figure Section 3: .28: Residuals Showing Wave Activity on Inbound Leg of Periapsis 056

Section 4: Conclusions

Aerobraking has proven to be an effective alternative to traditional means for decreasing the altitude of an orbiting satellite. Mars Global Surveyor has been aerobraking since September 1997, decreasing the period of the orbit from over 48 hours to under 20 hours. This has saved a significant amount of fuel, which in terms of launch cost, saves a significant amount of money. However, as expected, the lack of knowledge of the Martian atmosphere has led to increased risk for the mission. The large atmospheric disturbance on Periapsis 15 significantly altered the mission plan, endangering the spacecraft and leading to increased cost.

By using the spacecraft accelerometers, the GWU/JIAFS accelerometer team has aided the aerobraking process. Quick and accurate models of the atmosphere have aided the flight team in monitoring the atmosphere and ensuring spacecraft safety. This was made possible by the modeling and characterization addressed in this paper. Using the method of least squares on variants of the hydrostatic equation has proved an effective means of modeling the atmosphere to aid in aerobraking. The simple constant temperature model was effectively used by breaking the accelerometer data up into specific regions of interest and characterizing those regions. This led to knowledge at critical points such as periapsis altitude and the reference altitude. Knowledge at periapsis is crucial because this is the region of maximum density, and consequently the region that most threatens spacecraft safety. The reference altitude is an arbitrary point used to compare various orbits. With sufficient amounts of data, it is also possible to model the atmosphere with more complex models, which leads to more accurate information about the atmosphere. This is seen by the decrease in the standard deviation of the fits as the more complex models are used. But, the downside to these models is their lower probability of convergence. Another benefit seen with greater amounts of data is that the atmosphere can be modeled to higher altitudes. This was seen when eight times the amount of accelerometer data was returned soon after the aerobraking hiatus.

Once the aerobraking mission began, it became apparent that it was also necessary to have the ability to model the latitudinal variation. This was necessary to characterize the occasionally strong latitudinal variation that often signaled the approach of an atmospheric disturbance. This was done by adding a term to the existing models. As the mission continues, it may be advantageous, or even necessary, to add further parameters to the least squares models. By doing this, atmospheric characteristics can be predicted or determined better and better.

Furthermore, the modeling done by the GWU/JIAFS accelerometer team has increased the overall knowledge of the Martian atmosphere. This has led to the ability to more accurately predict atmospheric conditions for future orbits. Again, this reduces mission risk and enhances aerobraking effectiveness. And not only will this information aid the MGS mission, but can aid in mission planning for future Mars missions.

For future missions, another way to increase atmospheric model accuracy is by tailoring accelerometers to the aerobraking mission. Early identification of the need to use accelerometer data for atmospheric modeling will be important. By doing this, it is possible to specify the amount and type of data that will most effectively help model the

atmosphere. This can make aerobraking an extremely viable option for orbital maneuvers on future space flights.

Works Consulted

1. Bougher, S. and G. M. Keating, Neutral Upper Atmospheres of Venus and Mars, *Adv. Space Res.*, 7, No. 12, 57, 1987.

2. Burden, R. L. and J. D. Faires, *Numerical Analysis*, Boston: PWS, 1993, pp 437-459.

3. Hanson, W. B. and A. J. Stewart, Mars' Upper Atmosphere: Mean and Variations, *Adv. Space Res.*, 7, 87, 1982.

4. Hobbs, P. V. and J. M. Wallace, *Atmospheric Science: An Introductory Survey*, New York: Academic Press, 1977.

5. Keating, G. M., J. Y. Nicholson III, and L. R. Lake, Venus Upper Atmosphere Structure, *J. Geophys. Res.*, 85, 7941, 1980.

6. Kirk, D. B. and A. Seiff, Structure of the Atmosphere of Mars in Summer at Mid-Latitudes, *J. Geophys. Res.*, 82, 4364, 1977.

7. Seiff, A., Structure of the Atmospheres of Mars and Venus Below 100 Kilometers, *Adv. Space Res.*, 7, No. 12, 5, 1987.

8. Stein, J. A. and J. C. G. Walker, Models of the Upper Atmosphere for a Wide Range of Boundary Conditions, *J. Atmos. Sci.*, 22, 11, 1965.

9. Walker, J. C. G., Analytic Representation of Upper Atmosphere Densities Based on Jacchia's Static Diffusion Models, *J. Atmos. Sci.*, 22, 462, 1965.

10. http://mpfwww.jpl.nasa.gob/mgs/overvu/mplan/mplan.html